

Design high voltage gain DC converter based on maximum power point resistance for photovoltaic applications

Ibraheem Jawad Billy, Jasim Farhood Hussein

Department of Electrical Engineering, College of Engineering, University of Technology, Baghdad, Iraq

Article Info

Article history:

Received Aug 23, 2022

Revised Nov 2, 2022

Accepted Jan 10, 2023

Keywords:

Current-ripple

DC to DC converter

High voltage gain

Maximum power point as resistance

Switches voltage stress

ABSTRACT

Due to the nonlinear properties of photovoltaic (PV) modules, the design of the high-gain direct current (DC) converter for maximum power point tracking (MPPT) is complicated. In this paper, the design of a new step-up DC converter for MPPT applications is proposed. The proposed converter is structured of two symmetrical reverse-parallel DC-DC boost converters. This structure is supported by voltage multiplier cells equipped to increase output voltage and decrease voltage stress on semiconductor switches. To simplify the high-gain DC converter design, the PV module's maximum power point is treated as resistance by using the incremental conductance (INC) method. The MPPT boost converter's inductance, input capacitance, and output capacitance are calculated using the derived equations using nine parameters. The results showed that the proposed DC converter simulation meets the necessary requirements. The size of the input capacitor, inductor, and output capacitor have been decreased. When the proposed converter is compared to a traditional converter, there is less voltage stress, low current ripple, and an increase in voltage gain. This has led to an improvement in the overall converter efficiency.

This is an open access article under the [CC BY-SA](https://creativecommons.org/licenses/by-sa/4.0/) license.



Corresponding Author:

Ibraheem Jawad Billy

Department of Electrical Engineering, College of Engineering, University of Technology

Baghdad, Iraq

Email: eee.20.28@grad.uotechnology.edu.iq

1. INTRODUCTION

The photovoltaic (PV) module's maximum power is acquired using the MPPT converter. The MPPT converter is composed of three components: the power converter, the controlling device for the power converter, and the MPPT method. Over the years, researchers have created a number of different forms of the MPPT approach [1]-[3]. Included in this are the hill climbing method, also known as the incremental conductance (INC) method, the particle swarm optimization method, the perturb and observe method, and several more approaches.

The MPPT method's purpose is to locate the PV module's MPP. The output of the MPPT technique is frequently either the voltage reference or the duty cycle. Pulse width modulation (PWM) and the duty cycle generated by the MPPT technique are interconnected. While a voltage reference generated using the MPPT approach is sent into the power converter's controller. The MPPT converter's proportional-integral (PI) controller is both a normal and unconventional controller for the power converter [4]-[6] as well as a fuzzy logic controller, respectively. The MPPT converter's power converter also uses a buck converter [7], the boost converter [8], [9] the buck-boost converter [5], and the single-ended primary-inductor converter (SEPIC) [10]. The PV module serves as the typical input source for the power converter utilized for the MPPT converter, which functions using the switching pulses generated by the PWM.

To calculate the inductance and capacitance employed in the MPPT converter, the power converter is designed. For the controller to keep its output steady, it's crucial to maintain continuous current mode. In the discontinuous current mode, the MPPT converter activates if the inductance is too low. The MPPT converter grows bulky and has a delayed transient response if the inductance is too high. To guarantee that the voltage ripple is kept within the appropriate standard, the capacitance is computed.

The voltage ripple increases if the capacitance is too low. The MPPT converter's response time slows down if the capacitance is too high. The study undertaken is primarily focused on the development of the MPPT technique rather than the power converter design, which is often not the major emphasis of the MPPT converter development. On the other hand, development on the power system for the MPPT converter is still ongoing [6], [11]-[13]. Designing a novel power converter architecture for the MPPT converter is the study's main objective. Analyzing the correlation between the PV resistance, output resistance, and duty cycle is one of the study projects (Rmp-RL-D) [6], [11]. Based on the load and the PV module, this study chooses the power converter that is best for the MPPT converter. Analyzing the MPPT converter as a variable resistance emulator is part of another study on the power converter for the MPPT converter [13], however, their study does not provide a calculation of the inductance and capacitance for the MPPT converter. The MPPT converter applies the boost converter [14]-[16]. For the MPPT converter, the input capacitor must be connected in parallel with the boost converter's input source. According to study, without an input capacitor, the boost converter cannot operate at the PV module's maximum power point [17]-[19].

The goal of this paper is to consider ways to produce a new converter that has high operational performance such as high voltage gain, minimal voltage stress on component devices, very low input current ripple, and high efficiency. The 81 W PV module is simulated using the single diode model. The MPPT method used for the simulation is the incremental conductance method. By contrasting the theoretical result calculated from the resulting equation with the MPPT high gain direct current (DC) converter simulation data acquired from MATLAB/Simulink, the derivation is demonstrated.

2. MODELING OF PV COMPONENT PARTS

The PV model's idea is to build the PV module's current-voltage I-V curve. The single diode model, a representation of an electrical circuit, is the foundation for the PV model that is employed, as shown in Figure 1. Kirchhoff current law is used to construct the equation for the PV current, I_{pv} as illustrated in (1), [20]. It must be solved using an iteration approach because it is an implicit equation. Newton-Raphson technique iterations are used to resolve (1) [21].

$$I_{pv} = I_{ph} - I_s \cdot \left(e^{\frac{q \cdot (V_{pv} + I_{pv} R_s)}{AKT}} - 1 \right) - \frac{V_{pv} + I_{pv} R_s}{R_{sh}} \quad (1)$$

Where I_{pv} represents the photocurrent, I_s the dark current saturated, PV module voltage is denoted by V_{pv} . The series resistance is denoted by R_s (Ω). A is the ideality criterion. Boltzmann's constant, K is (1.38×10^{-23} J/K), T represent the p-n junction's temperature (K). q is the charge on an electron (1.6×10^{-19} C). Additionally, R_{sh} is the parallel resistance (Ω), I_{ph} is determined by [22]. While I_s is determined using (3) and just depends on temperature [23]. The maximum power point generated by the PV model is impacted by R_s and R_{sh} .

$$I_{ph} = \frac{G}{G_{STC}} \cdot (I_{sh} + K_i(T - T_{STC})) \quad (2)$$

$$I_s = \frac{(I_{sc} + K_i(T - T_{STC}))}{e^{\left(\frac{V_{oc} + \frac{K_v(T - T_{STC})}{AV_t}}{AV_t} \right) - 1}} \quad (3)$$

Where STC represents for the normal test condition (1000 W/m^2 and 25°C) and G is the irradiance (W/m^2). The temperature under STC is T_{stc} (25°C).

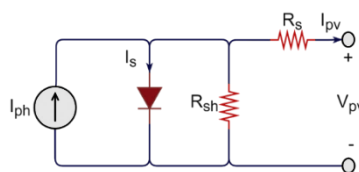


Figure 1. PV module circuit

2.1. Incremental conductance method for MPPT

The INC method is simple to use and does not need a power converter controller. The INC method immediately calculates the duty cycle [24]. The INC algorithm receives input from the PV array's voltage and current sensors [25]. The duty ratio D of the proposed converter is determined by this algorithm affected by changes in voltage, current, and power.

Figure 2 illustrates the nonlinear ring P_{PV} vs V_{PV} characteristics of a solar PV array. The operating point fluctuates depending on the load's impedance when applied to the array terminals. The P-V curve's operation point is tracked using a proposed DC-DC converter. The slope of the MPP curve is negative on the right side and positive on the left side. The slope of the curve is zero when the array is transferring its maximum possible power. The slope of the MPP curve is negative on the right side, and positive on the left side.

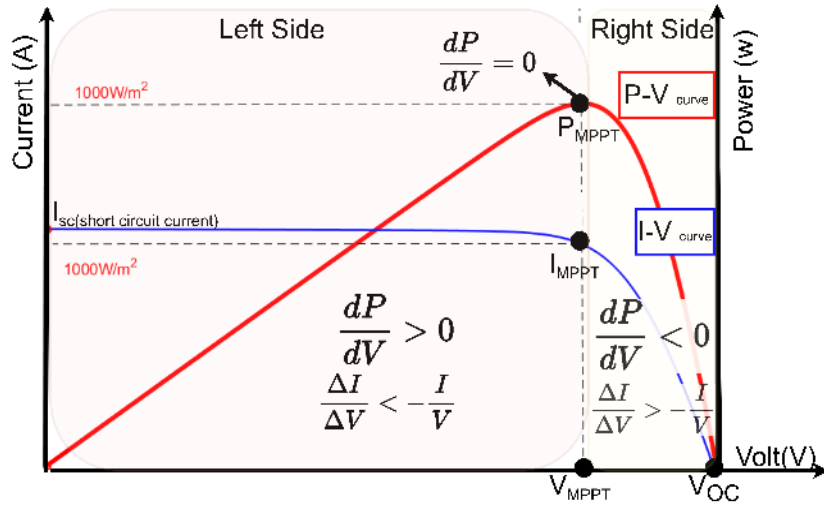


Figure 2. P vs. V and I vs. V curves for the solar PV array

The slope of the curve is zero when the array is transferring its maximum possible power. When a power equation is taken in to consideration and differentiated in relation to voltage, relationships between an INC and conductance are found for various portions of the curve as (4) and (5):

$$P_{pv} = I_{pv} \cdot V_{pv} \quad (4)$$

$$\frac{dP_{pv}}{dV_{pv}} = \frac{d(I_{pv} \cdot V_{pv})}{dV_{pv}} = I_{pv} + V_{pv} \cdot \frac{dI_{pv}}{dV_{pv}} \quad (5)$$

At MPPT:

$$\frac{dP_{pv}}{dV_{pv}} = 0; \frac{dI_{pv}}{dV_{pv}} = -\frac{I_{pv}}{V_{pv}} \quad (6)$$

At left side form P-V curve:

$$\frac{dP_{pv}}{dV_{pv}} > 0; \frac{dI_{pv}}{dV_{pv}} > -\frac{I_{pv}}{V_{pv}} \quad (7)$$

At right side form P-V curve:

$$\frac{dP_{pv}}{dV_{pv}} < 0; \frac{dI_{pv}}{dV_{pv}} < -\frac{I_{pv}}{V_{pv}} \quad (8)$$

The INC method depicted in Figure 3 is used to change the proposed converter's duty ratio.

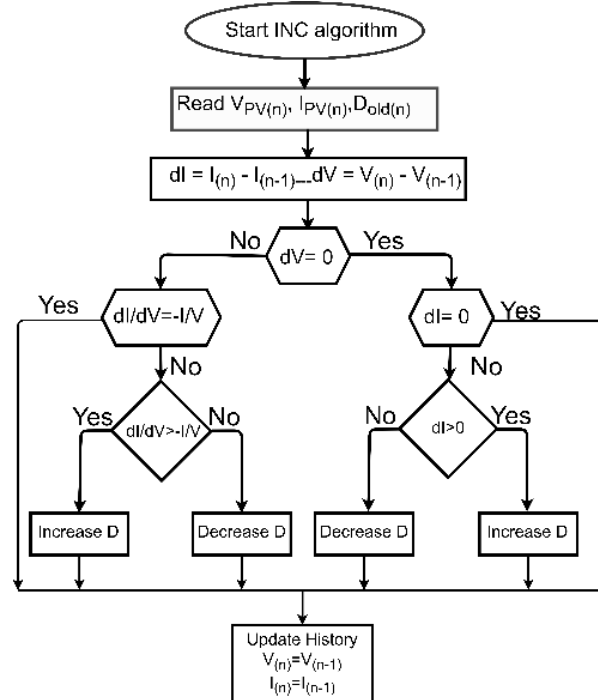


Figure 3. Flowchart of the INC method

3. MAXIMUM POWER POINT TRACKING BY HIGH STEP-UP DC CONVERTER

Figure 4 shows the proposed converter topology, which includes two inductors at the input source utilizing interleaving technical to reduce source current ripple, and two voltage multiplier units to boost output voltage. The switches are turned ON and OFF in the specified intervals. These waveforms as shown in Figure 5 are analyzed in this study as two square waves by the identical duty cycle and 180° phase difference; hence, the source current ripple and the input filter's volume might be drastically reduced. Each side of the proposed converter is a conventional converter connected in series with a voltage multiplier. Each switching capacitor-diode circuit boosts the output voltage of one side of these converters.

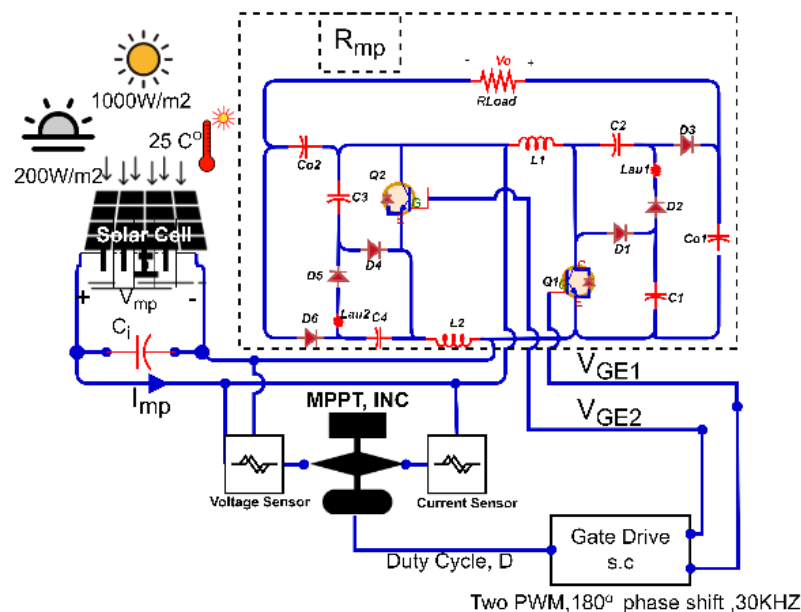


Figure 4. The schematic of the PV panel with the proposed converter

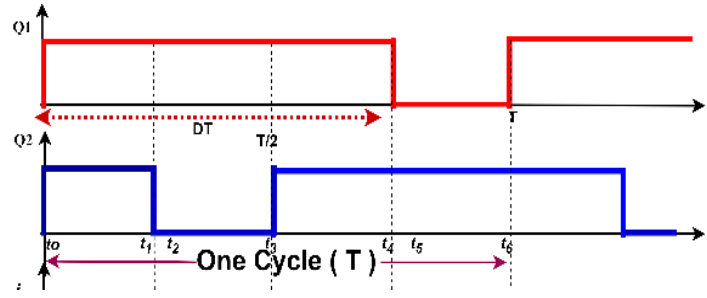


Figure 5. The gate drive waveforms for proposed converter's switch

3.1. Analysis of proposed converter in steady-state

3.1.1. Circuit modes

The proposed converter operates with a high conversion ratio there for the switches Q1 and Q2 are driven by turning ON and OFF in the specified intervals with a 180° phase difference, and a duty cycle greater than 0.5 as shown in Figure 5. Mode 1: $t_0 \leq t \leq t_1$: duration operation in this mode is considered by $(D-0.5)T$ as shown in Figure 5. Both switches Q1 and Q2 of the proposed converter are turned ON, and the energy increases both inductors L1 and L2, where the voltage input is applied to two inductors L1 and L2. Mode 1 is indicated in Figure 6(a).

$$V_{L1} = V_{mp} \quad (9)$$

$$V_{L2} = V_{mp} \quad (10)$$

Mode 2: $t_1 \leq t \leq t_2$: duration operation in this mode is considered by (dT) as shown in Figure 5. Switch Q1 is continue turned ON and switch Q2 is turned OFF, the energy continues to increase in the inductor L1 and decreases in the inductor L2. Mode 2 is indicated in Figure 6(b).

$$V_{L1} = V_{mp} \quad (11)$$

$$V_{L2} = V_{mp} - V_{C3} \quad (12)$$

Mode 3: $t_2 \leq t \leq t_3$: duration operation in this mode is considered by $[1-(D+d)]T$, Q1 is remain turned ON, Q2 is remain turned OFF, and D5 is reverse biased. Mode 3 is indicated in Figure 6(c).

$$V_{L1} = V_{mp} \quad (13)$$

$$V_{L2} = V_{mp} - V_{C3} \quad (14)$$

Mode 4: $t_3 \leq t \leq t_4$: duration operation in this mode is considered by $(D-0.5)T$ as shown in Figure 5, this mode is similar to mode 1. Mode 4 is indicated in Figure 6(d).

$$V_{L1} = V_{mp} \quad (15)$$

$$V_{L2} = V_{mp} - V_{C3} \quad (16)$$

Mode 5: $t_4 \leq t \leq t_5$: duration operation in this mode is considered by (dT) as shown in Figure 5. Switch Q1 is turned OFF, and switch Q2 is continue turned ON, and the energy continues to increase in the inductor L2 and decreases in the inductor L1. Mode 5 is indicated in Figure 6(e).

$$V_{L1} = V_{mp} - V_{C1} \quad (17)$$

$$V_{L2} = V_{mp} \quad (18)$$

Mode 6: $t_5 \leq t \leq t_6$: Duration operation in this mode is considered by $(1-(D+d))T$ as shown in Figure 5, switch Q1 is remain turned OFF, and switch Q2 is remain turned ON. Mode 6 is indicated in Figure 6(f).

$$V_{L1} = V_{mp} - V_{C1} \quad (19)$$

$$V_{L2} = V_{mp} \quad (20)$$

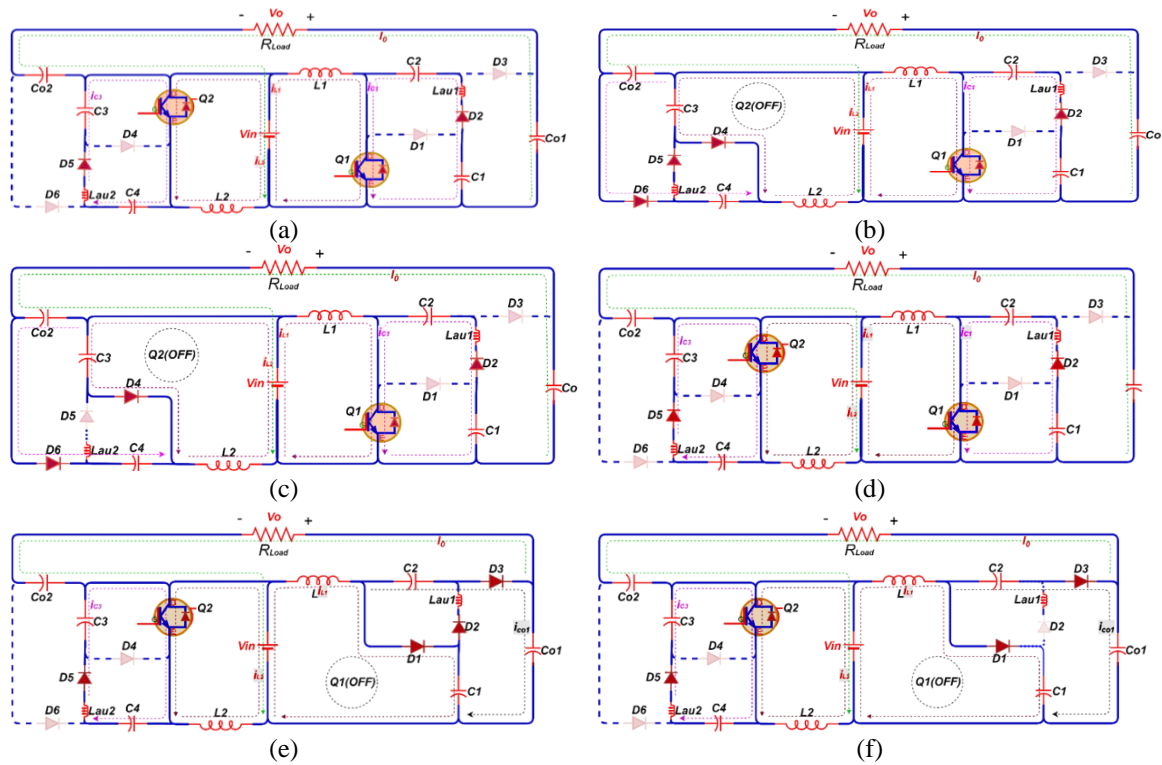


Figure 6. Circuit modes (a) mode 1, (b) mode 2, (c) mode 3, (d) mode 4, (e) mode 5, and (f) mode 6

3.2. Voltage gain derivation

Based on the principle of the balance of the voltage second, for the inductors' (L1, Lau1, L2, and Lau2), can be calculated capacitors C1 and C2 voltages can be obtained as (21)-(23):

$$V_{C1} = \frac{V_{mp}}{1-D} \quad (21)$$

$$V_{C2} = \frac{D}{d+D} \cdot V_{C1} \quad ; d \ll D \quad (22)$$

$$V_{C1} \approx V_{C2} = \frac{V_{mp}}{1-D} \quad (23)$$

The capacitors C3 and C4 voltages can be obtained as (24)-(26):

$$V_{C3} = \frac{V_{mp}}{1-D} \quad (24)$$

$$V_{C4} = \frac{D}{d+D} \cdot V_{C3} \quad ; d \ll D \quad (25)$$

$$V_{C4} \approx V_{C3} = \frac{V_{mp}}{1-D} \quad (26)$$

By using Kirchhoff's voltage law in the cycle $V_{C1} - V_{C2} - V_{Co1}$:

$$V_{Co1} = V_{C1} + V_{C2} = \frac{2V_{in}}{1-D} \quad (27)$$

By using Kirchhoff's voltage law in the cycle $V_{C3}-V_{C4}-V_{CO2}$:

$$V_{CO2} = V_{C3} + V_{C4} = \frac{2V_{in}}{1-D} \quad (28)$$

By using Kirchhoff's voltage law in the cycle $V_{in}-V_{CO1}-V_O-V_{CO2}$:

$$\frac{V_O}{V_{mp}} = \frac{3+D}{1-D} \quad (29)$$

The voltage and current at maximum power point (V_{mp} and I_{mp}) are used to compute the maximum power point resistance R_{mp} :

$$R_{mp} = \frac{V_{mp}}{I_{mp}} \quad (30)$$

Only under specific conditions can the MPPT proposed converter achieve the appropriate system needs. The intended operational region, ADO, where this condition occurs at different irradiances G , is depicted in Figure 7. These two MPPs are converted into R_{mp} using (30).

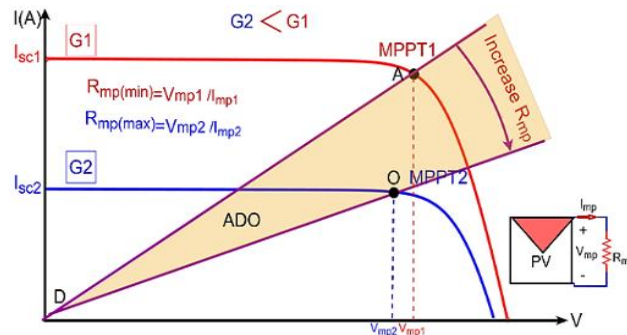


Figure 7. PV's I-V typical curve at various irradiances

3.3. Load resistance calculation

For lossless power DC converter, the input power equals to the output power:

$$P_{in} = P_o \quad (31)$$

$$V_{mp} \cdot I_{mp} = \frac{V_o^2}{R_L} \quad (32)$$

$$R_L = R_{mp} \cdot \left(\frac{3+D}{1-D} \right)^2 = R_{mp} \cdot M_{prop}^2 \quad (33)$$

The minimum of R_L during the lowest irradiance is given by:

$$R_{L(min)} = R_{mp(max)} \cdot \left(\frac{3+D_{min}}{1-D_{min}} \right)^2 = R_{mp(max)} \cdot M_{prop(min)}^2 \quad (34)$$

The maximum of R_L during the highest irradiance is given by:

$$R_{L(max)} = R_{mp(min)} \cdot \left(\frac{3+D_{max}}{1-D_{max}} \right)^2 = R_{mp(min)} \cdot M_{prop(max)}^2 \quad (35)$$

If a fixed load resistance value is employed, the optimal load resistance, R_L , is crucial.

$$R_{mp(max)} \cdot M_{prop(min)}^2 \leq R_L \leq R_{mp(min)} \cdot M_{prop(max)}^2 \quad (36)$$

3.4. Output voltage ripple calculation and output capacitance design

The output voltage is at its maximum value at maximum load resistance and maximum duty cycle.

$$V_O = V_{mp} \cdot \sqrt{\frac{R_L}{R_{mp}}} \quad (37)$$

$$V_{O(max)} = V_{mp(G1)} \cdot \left(\frac{3+D_{max}}{1-D_{max}} \right) \quad (38)$$

The output voltage ripple factor (γ_{Vo}) can be calculated:

$$\gamma_{Vo} = \frac{\Delta V_O}{V_O} = \frac{D}{R_L \cdot C_O \cdot f_s} \quad (39)$$

$$\gamma_{Vo} = \frac{D \cdot (1-D)^2}{R_{mp} \cdot (3+D)^2 \cdot C_O \cdot f_s} \quad (40)$$

At duty cycle $D = 0.3$, the maximum output voltage ripple factor for variable load occurs when $\frac{d}{dD} \cdot \gamma_{Vo} = 0$. Then the maximum ripple factor from (40) becomes:

$$\gamma_{Vo_{max}} = \frac{0.0135}{R_{mp} \cdot C_O \cdot f_s}; \quad \text{at } D = 0.3 \quad (41)$$

From (33) at $D = 0.3$. The maximum output voltage ripple factor occurs when the load's resistance R_L equals 22.25 times from maximum power point resistance R_{mp} . The output capacitances may be calculated using (42):

$$C_{o_{min}} = C_{o1_{min}} = C_{o2_{min}} = \frac{0.0135}{R_{mp} \cdot \gamma_{Vo(max)} \cdot f_s} \quad (42)$$

3.5. Inductance design

The inductance of the proposed converter, L is given in (43):

$$L = L_1 = L_2 = \frac{V_{mp} \cdot D}{\Delta I_L \cdot f_s} \quad (43)$$

Where V_{mp} represent the input voltage source. The ripple inductor current can be calculated by product ripple factor with an average current of the inductor $\Delta I_L = \gamma_L \cdot I_L$ where the average current is given in (44):

$$I_L \approx \frac{I_{mp}}{2} \quad (44)$$

where I_{mp} represent the input current at maximum power point, from (44) and (45) the inductance value is:

$$L = \frac{2 \cdot R_{mp} \cdot D}{\gamma_L \cdot f_s}; \quad \text{where} \quad f_s = \frac{1}{T}; \quad \gamma_L = \frac{\Delta I_L}{I_L} \quad (45)$$

From (33) and (45):

$$\gamma_L = \frac{R_L \cdot D \cdot (1-D)^2}{L \cdot f_s \cdot (3+D)^2} \quad (46)$$

From (46) the minimum inductance accrues when γ_L at maximum value, therefore $\frac{d\gamma_L}{dD} = 0$. To find the duty cycle value to make γ_L at a maximum value:

$$\frac{d\gamma_L}{dD} = 0 = \frac{R_L \cdot L \cdot f_s \cdot [(3+D)^2 \cdot (3D^2 - 4D + 1) - 2 \cdot D \cdot R_L \cdot L \cdot f_s \cdot (1-D)^2 \cdot (3+D)]}{[L \cdot f_s \cdot (3+D)^2]^2} \quad (47)$$

From (47) the duty cycle $D = 0.3$. The maximum value of the R_{mp} occur when its value equal to $0.045R_L$ by substituting $D = 0.3$, in (33). The critical inductance by substituting $D = 0.3$, in (46):

$$L_{crit} = 0.0135 \cdot \frac{R_L}{\gamma_{L_{max}} \cdot f_s} \quad (48)$$

3.6. Input capacitance design

The input current ripple, which is the flow in the input capacitor C_i as shown in Figure 4. The change in charge in this capacitor can be calculated by shading area as shown in Figure 8.

$$\Delta Q = \frac{1}{2} \cdot \left(\frac{T}{4}\right) \cdot \left(\frac{\Delta I_{in}}{2}\right) = \frac{\Delta I_{in}}{16 \cdot f_s} \quad (49)$$

The input current ripple is:

$$\Delta I_{in} = \Delta I_{mp} = \frac{V_{mp} \cdot (2D-1)}{f_s \cdot L} \quad (50)$$

According to the concept of capacitance, the connection between the maximum power point voltages ripple ΔV_{mp} and ΔQ is:

$$\Delta V_{mp} = \frac{\Delta Q}{C_i} \quad (51)$$

The maximum power point voltage ripple is:

$$\Delta V_{mp} = \gamma_{V_{mp}} \cdot V_{mp} \quad (52)$$

Where $\gamma_{V_{mp}}$ is the maximum power point voltage ripple factor.

From (49)-(52) the input capacitor is:

$$C_i = \frac{2D-1}{16 \cdot \gamma_{V_{mp}} \cdot L \cdot f_s^2} \quad (53)$$

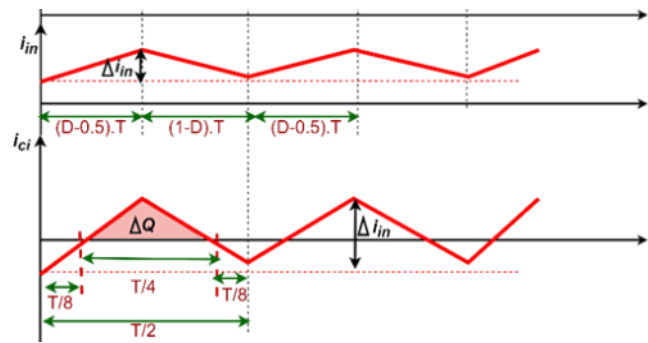


Figure 8. The input capacitor current charge for the proposed converter

4. SIMULATION OF THE PROPOSED CONVERTER WITH A PV SOLAR CELL

The MPPT proposed converter's maximum load resistance R_{Lmax} is constrained by D_{max} . Lower R_{Lmax} is the result of lower D_{max} . The output voltage V_o should rise as the duty cycle D rises in perfect condition. On the other hand, in reality, the output voltage V_o only rises so far at the limit point where it is decreased as the duty cycle D is increased beyond the normal limit. In addition, the load resistance and duty cycle, R_L , D_{max} have an impact on the MPPT proposed converter's effectiveness. Lower efficiency is the result of a greater D_{max} . This is because conduction losses have risen. D_{max} is suggested in the simulation to be 60%. The parameters listed in Table 1 and 81 W PV as shown in Figure 9 is used to regulate it at MPPT proposed converter. Table 2 illustrates how L and C_i vary depending on the R_L state. L decreases as $R_{L(max)}$ lower. Since C_i is influenced by L , C_i rises when L falls to keep $\gamma_{V_{mp}}$ constant.

Figure 10 depicts the relation between output resistance and irradiance. The range of R_L gets smaller as the irradiance rises. The output resistance range for 200 W/m² is between 218.3 Ω and 1,490 Ω. But, when 1000 W/m² is applied, the range is between 43 Ω to 294 Ω. To avoid the MPPT proposed converter from running beyond the duty cycle range, the minimum and maximum R_L are applied.

As seen in Figures 11(a) and (b) when maximum R_L is employed, the system typically works at D_{max} ($D_{max} = 0.6$), where the systems work at D_{min} when the minimal R_L is applied to the MPPT proposed converter ($D_{min} = 0.1$). When the irradiance changes, R_L is frequently altered to keep the duty cycle from going extremely low or high. Fixed load $R_{L(cons.)}$ is made to operate between D_{min} and D_{max} , using $R_{L(cons.)}$ eliminates the need to change load. This is due to the higher cost of a variable resistor used to express the variation load than a constant load used to represent $R_{L(cons.)}$.

Table 1. The variables needed to compute the MPPT proposed converter's component

Parameters	Variables	Value
PV module	Maximum power point ($V_{mp}(V), I_{mp}(A)$) for high irradiance (1000 W/m^2)	$V_{mp} = 17.42 \text{ V}; I_{mp} = 4.63 \text{ A}$ $R_{mp} = \frac{V_{mp}}{I_{mp}} = 3.76 \Omega$
	Maximum power point ($V_{mp}(V), I_{mp}(A)$) for low irradiance (200 W/m^2)	$V_{mp} = 17.3 \text{ V}; I_{mp} = 0.94 \text{ A}$ $R_{mp} = \frac{V_{mp}}{I_{mp}} = 18.4 \Omega$
	Ripple Factor (γ)	20%
	Inductor current ripple factor, γ_L (%)	0.12 %
Characteristic of (PWM)Technique	Maximum power point voltage ripple factor, $\gamma_{V_{mp}}$ (%)	0.12 %
	Output voltage ripple factor, γ_{V_o} (%)	0.12 %
	Minimum duty cycle limit, D_{min}	0.1
	Maximum duty cycle limit, D_{max}	0.6
Load	Switching frequency, f_s	30 KHZ
	Maximum load resistance, $R_{L(max)}$ (Ω)	For limit load, the maximum load resistance at low irradiance (200 W/m^2) $R_{o(max.g)} = 300 \Omega$

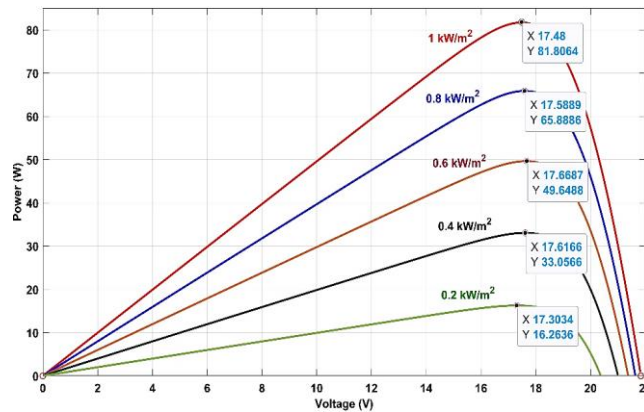


Figure 9. Solar PV module power–voltage (P-V) curves

Table 2. The elements needed in three different cases for the MPPT proposed converter

Load model	Variable load	Limit load	Constant load
Duty cycle D	$D_{min} \leq D \leq D_{max}$	$R_L \leq R_{L(max)}$	$R_{L(cons.)}$
Load resistance $R_L(\Omega)$	Low irradiance (200 W/m^2); $R_{L(min.g)} = R_{mp} \cdot \left(\frac{3 + D_{min}}{1 - D_{min}} \right)^2 = 218.3 \Omega$ $R_{L(max.g)} = R_{mp} \cdot \left(\frac{3 + D_{max}}{1 - D_{max}} \right)^2 = 1490$ High irradiance (1000 W/m^2); $R_{L(min.G)} = R_{mp} \cdot \left(\frac{3 + D_{min}}{1 - D_{min}} \right)^2 = 43$ $R_{L(max.G)} = R_{mp} \cdot \left(\frac{3 + D_{max}}{1 - D_{max}} \right)^2 = 294$	Low irradiance (200 W/m^2); $218.3 \leq R_L \leq 300$ High irradiance (1000 W/m^2); $43 \leq R_L \leq 294$	Average constant load between max load and min load for High and low irradiance $R_{L(cons.)} = \frac{300 + 43}{2} = 171.5$ OR between range $43 \leq R_{L(cons.)} \leq 300$
Inductance, $L(\text{mH})$	From (49) $L = \frac{0.0135 \cdot R_{L(max)}}{\gamma_L \cdot f_s} = 3.68$	$\frac{R_{L(limit)}}{R_{mp.g}} = \left(\frac{3 + D_{max}}{1 - D_{max}} \right)^2$ $= \frac{300}{18.4}; D_{max} = 0.2$ $L = \frac{V_{mp.g} \cdot D_{max}}{\gamma_L \cdot \frac{I_{mp.g}}{2} \cdot f_s} = 1.22$	For $R_{L(cons.)} = 300 \Omega$ $L = 0.0135 \cdot \frac{R_L}{\gamma_L \cdot f_s} = 0.67$
Output Capacitance, $C_{o max}(\mu\text{F})$	From (43) $C_{o min} = \frac{0.0135}{R_{mp} \cdot \gamma_{V_o(max)} \cdot f_s} = 100$	From (40) $C_{o min} = \frac{D}{R_L \cdot \gamma_{V_o} \cdot f_s} = 18.5$	From (40) $C_{o min} = \frac{D}{R_L \cdot \gamma_{V_o} \cdot f_s} = 55.45$
Input Capacitance, $C_{i min}(\mu\text{F})$	$C_{i(min)} = \frac{2D_{max} - 1}{16 \cdot \gamma_{V_{mp}} \cdot L \cdot f_s^2} = 3.145$	$C_i = \frac{2D_{max} - 1}{16 \cdot \gamma_{V_{mp}} \cdot L \cdot f_s^2} = 9.5$ $D_{max} = 0.6$	at $C_{i(min)} = \frac{2D_{max} - 1}{16 \cdot \gamma_{V_{mp}} \cdot L \cdot f_s^2} = 30$

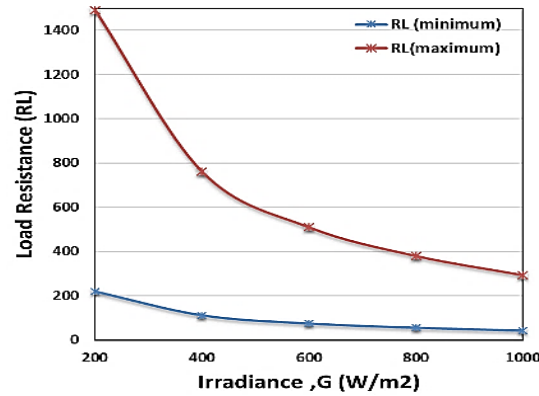


Figure 10. Load resistance with different irradiance

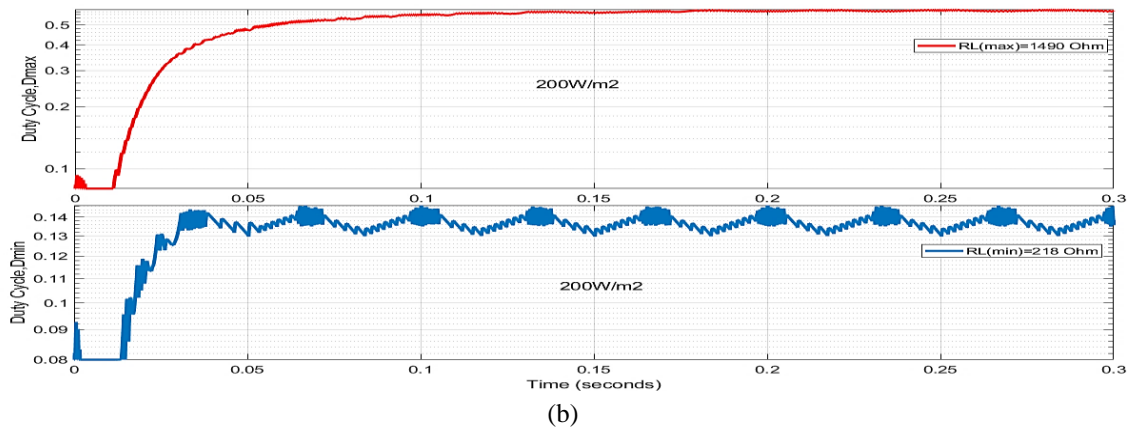
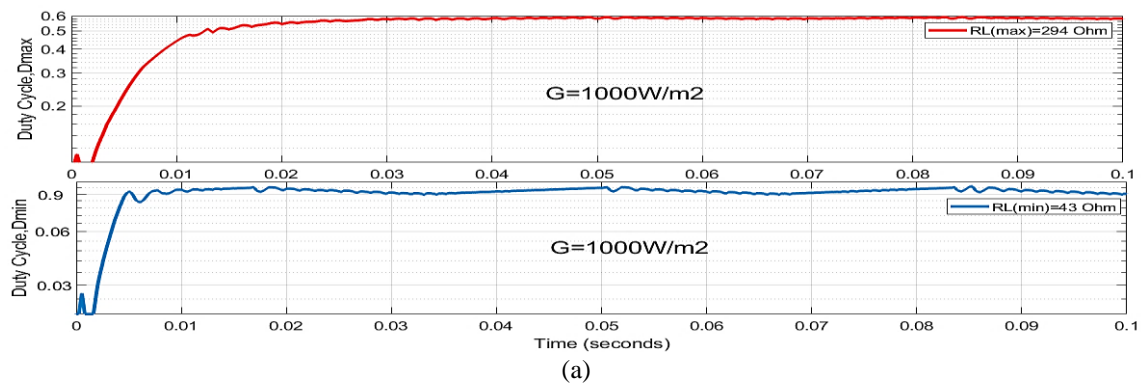
Figure 11. The duty cycle with the $R_{L(max)}$ and $R_{L(min)}$ (a) 1000 W/m^2 and (b) 200 W/m^2

Figure 12 illustrates for constant load. In comparison to the duty cycle for $1,000 \text{ W/m}^2$, which is maximum value $D_{max} = 0.6$, the duty cycle for $200 \frac{\text{W}}{\text{m}^2}$ is greater than D_{min} (0.1). Results indicate the duty cycle is in the acceptable duty cycle range. The MPPT proposed converter is tested under various situations, and the simulation's results are displayed in Figure 13. The simulation and theoretical γ_L results are very close, as illustrated in Table 3 and Figure 14. According to the simulations, γ_L is greatest when R_L is equal to $R_{L(max,g)}$ at low irradiation g .

In both theoretical and simulation cases, the output voltage ripple factor γ_{Vo} is 0.1 percent and 0.11 percent, respectively as shown in Figure 15 at load resistance $R_L = 100 \Omega$ and high irradiance $1,000 \text{ W/m}^2$ and it's very nearer to maximum value 0.12 percent which occurs at load resistance $R_L = 82.6 \Omega$ for theoretical calculation in Table 4 and in Figure 16. This establishes the accuracy of the calculated $C_{o(min)}$. Figure 17 shows the comparison between the theoretical calculation and simulation results for various output voltages with various load resistances and proves the accuracy of the equations used.

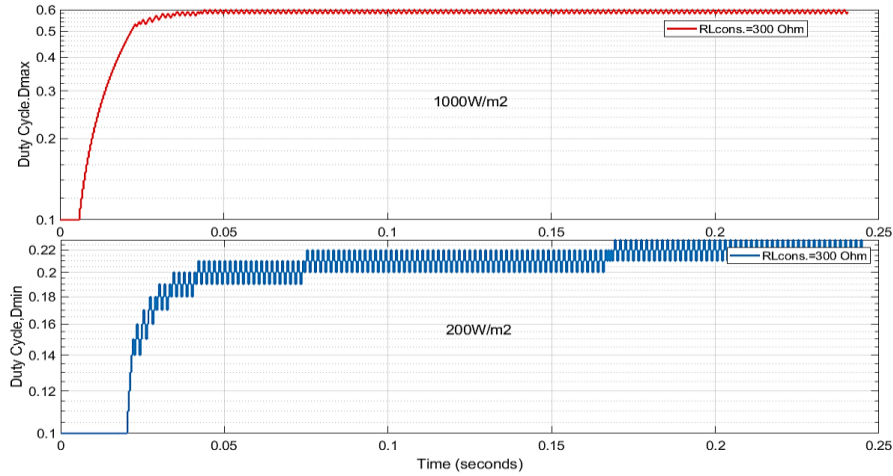


Figure 12. The duty cycle with the $R_{L(cons.)}$ with irradiance 1000 W/m^2 and 200 W/m^2

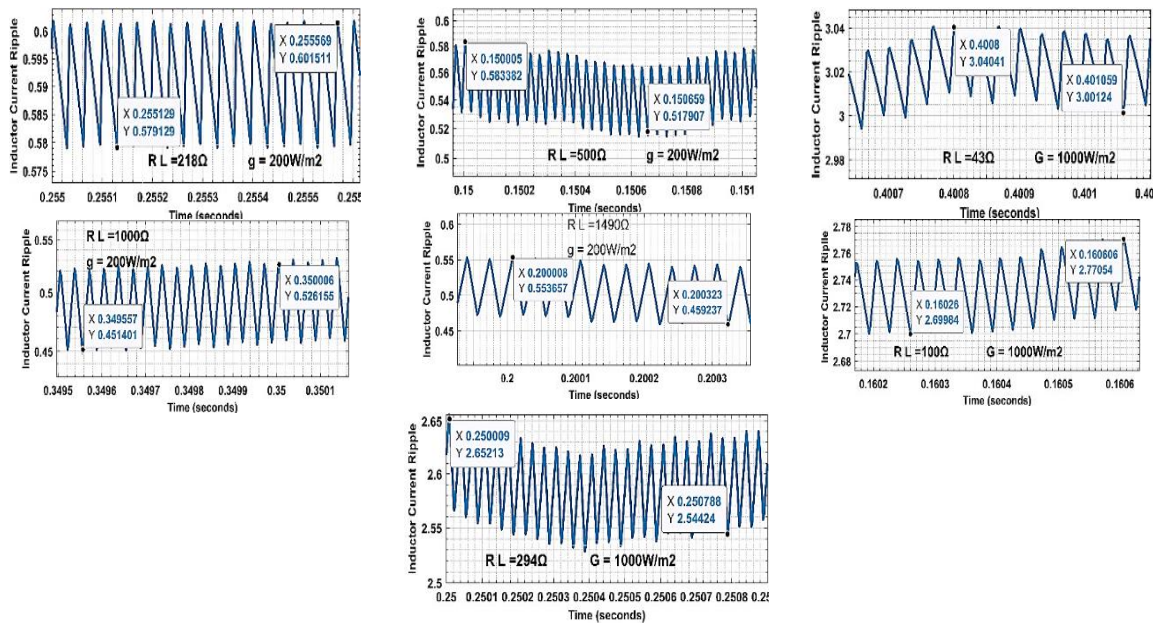


Figure 13. Inductors current ripple at various load resistance R_L and irradiance G

Table 3. The inductor current ripple factor is in both theoretical and simulation computations

Irradiance G	Variable load resistance $R_L (\Omega)$	Inductor current ripple factor γ_L % theoretically	Inductor current ripple factor γ_L % simulation result
1,000 W/m^2	43	$\gamma_L = \frac{2 \cdot R_{mp.G} \cdot D_G}{L \cdot f_s} ; R_{mp.G} = 3.76 \Omega$ $\left(\frac{3+D}{1-D} \right)^2 = \frac{R_L}{R_{mp.G}} ; D = 0.1$ $\gamma_L \% = 1.02$	From Figure 13 $\gamma_L \% = \frac{\text{peak to peak}}{\text{Mean}} = 1.27$
	100	2.38 at $D = 0.35$	2.6
	294	4 at $D = 0.6$	4.2
	218	$\gamma_L = \frac{2 \cdot R_{mp.g} \cdot D_{max.g}}{L \cdot f_s} R_{mp.g} = 18.4 \Omega$ $\left(\frac{3+D}{1-D} \right)^2 = \frac{R_L}{R_{mp.G}} ; D \approx 0.15$ $\gamma_L \% = 5$	4
200 W/m^2	500	11.86 at $D = 0.35$	11.5
	1,000	17.4 at $D = 0.5$	16
	1,490	19.98	18.9

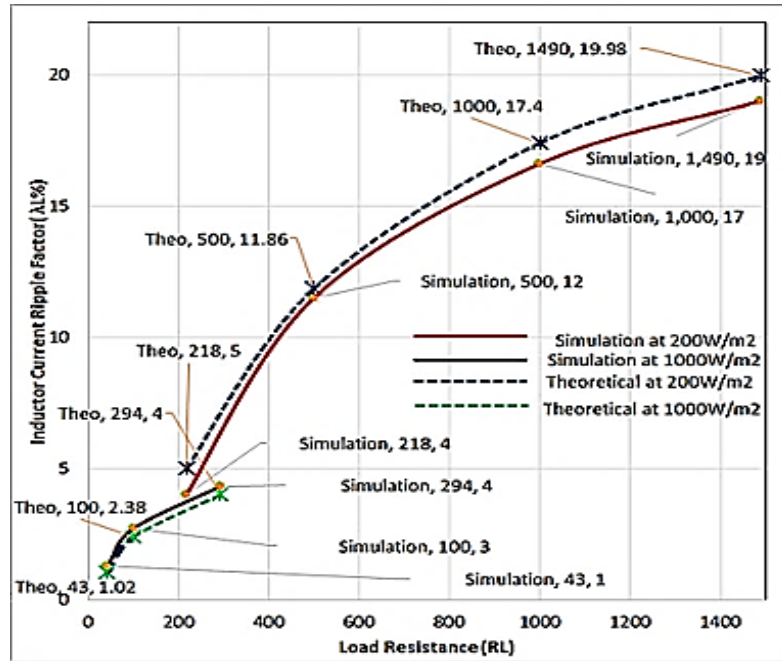


Figure 14. Comparison of inductor current ripple factor in theoretical and simulation results

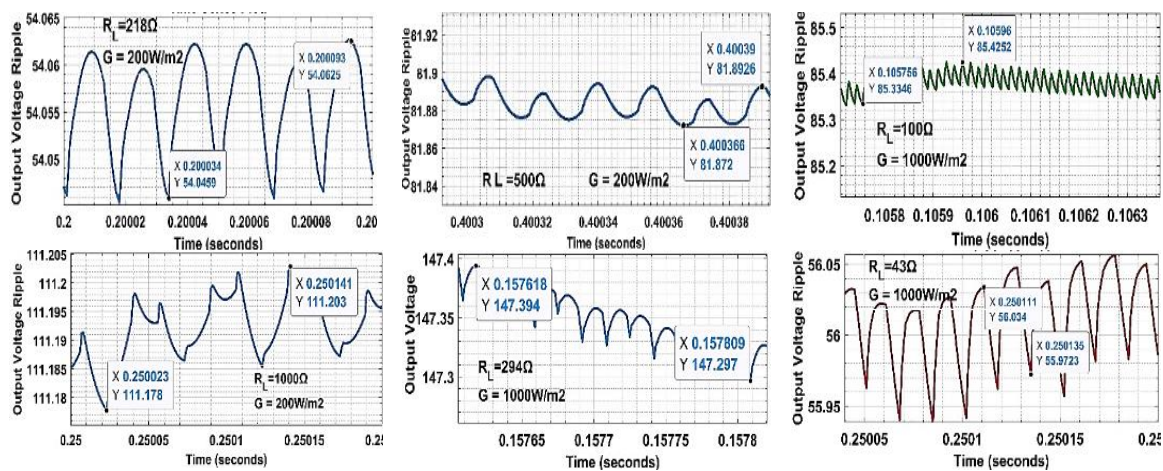
Figure 15. Output voltage ripple at various load resistance R_L and irradiance G

Table 4. The output voltage ripple factor is in both theoretical and simulation computations.

Irradiance G	Variable load resistance $R_L (\Omega)$	Output voltage ripple $\gamma_{Vo} \%$ factor theoretically	Inductor ripple factor $\gamma_L \%$ simulation result
1,000 W/m ²	43	$\gamma_{Vo} = \frac{D_G}{R_L \cdot C_o \cdot f_s} = 0.08$	$\gamma_{Vo} \% = \frac{\text{peak to peak}}{\text{Mean}} = 0.1$
	100	0.11 at $D = 0.35$ (near from the maximum ripple factor occurs at $D = 0.3$ when $R_L = 22.22$. $R_{mp} = 82.65 \Omega$)	2.6
	294	0.068	0.065
200 W/m ²	218	$\gamma_{Vo} = \frac{D_g}{R_L \cdot C_o \cdot f_s}$ $D_g \approx 0.15$; $\gamma_{Vo} \% = 0.023$	0.03
	500	0.024	0.024
	1000	0.0174	0.0174

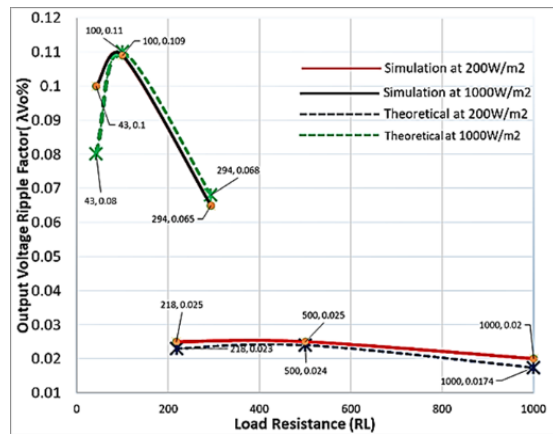


Figure 16. The ripple factor of the output voltage at various load resistances

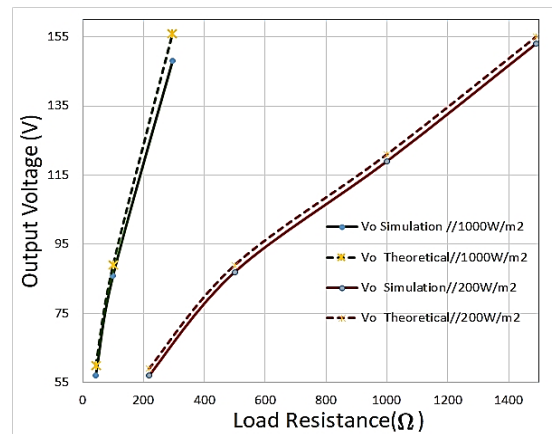


Figure 17. The accuracy result for the output voltage at various load resistances and irradiance

5. CONCLUSION

Making the converter reflect the total resistance detected by the PV module allowed for the derivation of the components for the MPPT DC converter. The output resistance, inductance, input capacitance, and output capacitance make up the components. With the use of this derivation, the MPPT boost converter's ripple factor and duty cycle may be adjusted to meet specific requirements. Additionally, the oversized system is eliminated, which results in a cheaper price and a smaller MPPT DC converter with a high gain ratio and low stress on all components. Given that the ideal condition is the one used in the derivation, a number of procedures must be followed to guarantee that the right minimum requirement is applied. The derivation is tailored for the PV application, resulting in a more straightforward and precise computation of the MPPT-proposed DC converter.




REFERENCES

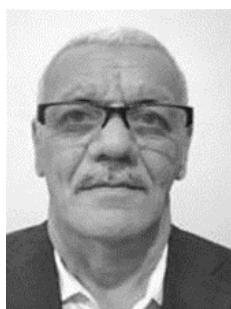
- [1] N. A. Kamarzaman and C. W. Tan, "A comprehensive review of maximum power point tracking algorithms for photovoltaic systems," *Renewable and Sustainable Energy Reviews*, vol. 37, pp. 585–598, Sep. 2014, doi: 10.1016/j.rser.2014.05.045.
- [2] N. Karami, N. Moubayed, and R. Outbib, "General review and classification of different MPPT Techniques," *Renewable and Sustainable Energy Reviews*, vol. 68, pp. 1–18, Feb. 2017, doi: 10.1016/j.rser.2016.09.132.
- [3] M. Seyedmahmoudian *et al.*, "State of the art artificial intelligence-based MPPT techniques for mitigating partial shading effects on PV systems—A review," *Renewable and Sustainable Energy Reviews*, vol. 64, pp. 435–455, Oct. 2016, doi: 10.1016/j.rser.2016.06.053.
- [4] J. Ahmed and Z. Salam, "An improved perturb and observe (P&O) maximum power point tracking (MPPT) algorithm for higher efficiency," *Applied Energy*, vol. 150, pp. 97–108, Jul. 2015, doi: 10.1016/j.apenergy.2015.04.006.
- [5] T. H. Kwan and X. Wu, "High performance P&O based lock-on mechanism MPPT algorithm with smooth tracking," *Solar Energy*, vol. 155, pp. 816–828, Oct. 2017, doi: 10.1016/j.solener.2017.07.026.
- [6] B. Nayak, A. Mohapatra, and K. B. Mohanty, "Selection criteria of dc-dc converter and control variable for MPPT of PV system utilized in heating and cooking applications," *Cogent Engineering*, vol. 4, no. 1, p. 1363357, Jan. 2017, doi: 10.1080/23311916.2017.1363357.
- [7] R. Balasankar, G. T. Arasu, and J. S. C. M. Raj, "A global MPPT technique invoking partitioned estimation and strategic deployment of P&O to tackle partial shading conditions," *Solar Energy*, vol. 143, pp. 73–85, Feb. 2017, doi: 10.1016/j.solener.2016.12.018.
- [8] A. Kchaou, A. Naamane, Y. Koubaa, and N. M'sirdi, "Second order sliding mode-based MPPT control for photovoltaic applications," *Solar Energy*, vol. 155, pp. 758–769, Oct. 2017, doi: 10.1016/j.solener.2017.07.007.
- [9] A. M. Palaniswamy and K. Srinivasan, "Takagi-Sugeno fuzzy approach for power optimization in standalone photovoltaic systems," *Solar Energy*, vol. 139, pp. 213–220, Dec. 2016, doi: 10.1016/j.solener.2016.09.027.
- [10] I. Pervez, I. Shams, S. Mekhilef, A. Sarwar, M. Tariq, and B. Alamri, "Most Valuable Player Algorithm based Maximum Power Point Tracking for a Partially Shaded PV Generation System," *IEEE Transactions on Sustainable Energy*, vol. 12, no. 4, pp. 1876–1890, Oct. 2021, doi: 10.1109/TSTE.2021.3069262.
- [11] M. E. Başoğlu and B. Çakır, "Comparisons of MPPT performances of isolated and non-isolated DC–DC converters by using a new approach," *Renewable and Sustainable Energy Reviews*, vol. 60, pp. 1100–1113, Jul. 2016, doi: 10.1016/j.rser.2016.01.128.
- [12] T. Bennett, A. Zilouchian, and R. Messenger, "Photovoltaic model and converter topology considerations for MPPT purposes," *Solar Energy*, vol. 86, no. 7, pp. 2029–2040, Jul. 2012, doi: 10.1016/j.solener.2012.04.005.
- [13] N. H. Baharudin, T. M. N. T. Mansur, F. A. Hamid, R. Ali, and M. I. Misrun, "Topologies of DC-DC Converter in Solar PV Applications," *Indonesian Journal of Electrical Engineering and Computer Science*, vol. 8, no. 2, Nov. 2017, doi: 10.11591/ijeecs.v8.i2.pp368-374.
- [14] J. Qi, Y. Zhang, and Y. Chen, "Modeling and maximum power point tracking (MPPT) method for PV array under partial shade conditions," *Renewable Energy*, vol. 66, pp. 337–345, Jun. 2014, doi: 10.1016/j.renene.2013.12.018.
- [15] R. Rajesh and M. C. Mabel, "Efficiency analysis of a multi-fuzzy logic controller for the determination of operating points in a PV system," *Solar Energy*, vol. 99, pp. 77–87, Jan. 2014, doi: 10.1016/j.solener.2013.10.036.




- [16] J. R-Hernanz, J. M. L-Guede, O. Barambones, E. Zulueta, and U. F-Gamiz, "Novel control algorithm for MPPT with Boost converters in photovoltaic systems," *International Journal of Hydrogen Energy*, vol. 42, no. 28, pp. 17831–17855, Jul. 2017, doi: 10.1016/j.ijhydene.2017.02.028.
- [17] M. Ding, Y. Tang, W. Cao, Z. Tan, Q. Wang, and D. Li, "Sliding Mode MPPT Controller for Photovoltaic Systems Under Partial Shading Conditions," *Journal of Advanced Computational Intelligence and Intelligent Informatics*, vol. 20, no. 7, pp. 1112–1118, Dec. 2016, doi: 10.20965/jaciii.2016.p1112.
- [18] S. R. Devireddy, S. Porpandiselvi, and B. Salvi, "A Fast GMPPT Algorithm for PV Array under Non-uniform Shading Conditions," in *2021 IEEE 18th India Council International Conference (INDICON)*, Dec. 2021, pp. 1–6, doi: 10.1109/INDICON52576.2021.9691625.
- [19] A. Vangari, D. Haribabu, and J. N. Sakamuri, "Modeling and control of DC/DC boost converter using K-factor control for MPPT of solar PV system," in *2015 International Conference on Energy Economics and Environment (ICEEE)*, Mar. 2015, pp. 1–6, doi: 10.1109/EnergyEconomics.2015.7235087.
- [20] M. Balato, L. Costanzo, D. Gallo, C. Landi, M. Luiso, and M. Vitelli, "Design and implementation of a dynamic FPAA based photovoltaic emulator," *Solar Energy*, vol. 123, pp. 102–115, Jan. 2016, doi: 10.1016/j.solener.2015.11.006.
- [21] A. Xenophontos, J. Rarey, A. Trombetta, and A. M. Bazzi, "A flexible low-cost photovoltaic solar panel emulation platform," in *2014 Power and Energy Conference at Illinois (PECI)*, Feb. 2014, pp. 1–6, doi: 10.1109/PECI.2014.6804542.
- [22] R. Kadri, H. Andrei, J.-P. Gaubert, T. Ivanovici, G. Champenois, and P. Andrei, "Modeling of the photovoltaic cell circuit parameters for optimum connection model and real-time emulator with partial shadow conditions," *Energy*, vol. 42, no. 1, pp. 57–67, Jun. 2012, doi: 10.1016/j.energy.2011.10.018.
- [23] V. J. Chin, Z. Salam, and K. Ishaque, "Cell modelling and model parameters estimation techniques for photovoltaic simulator application: A review," *Applied Energy*, vol. 154, pp. 500–519, Sep. 2015, doi: 10.1016/j.apenergy.2015.05.035.
- [24] D. Sera, L. Mathe, T. Kerekes, S. V. Spataru, and R. Teodorescu, "On the Perturb-and-Observe and Incremental Conductance MPPT Methods for PV Systems," *IEEE Journal of Photovoltaics*, vol. 3, no. 3, pp. 1070–1078, Jul. 2013, doi: 10.1109/JPHOTOV.2013.2261118.
- [25] R. Çelikel and A. Gündoğdu, "Comparison of PO and INC MPPT Methods Using FPGA In-The-Loop under Different Radiation Conditions," *Balkan Journal of Electrical and Computer Engineering*, vol. 9, no. 2, Apr. 2021, doi: 10.17694/bajece.884815.

BIOGRAPHIES OF AUTHORS



Ibraheem Jawad Billy    is a Master's Student at the College of Electrical Engineering, University of Technology and Baghdad, Iraq. He received a B.Sc. in Electrical Engineering from the University of Babylon, Iraq in 2006. He is currently working toward an M. Sc degree in Electrical Engineering at the University of Technology, Iraq. His research interest is in the area of DC-DC converters, controller design, and renewable energy. He can be contacted at email: eee.20.28@grad.uotechnology.edu.iq.



Dr. Jasim Farhood Hussein    received the B.Sc. in Electrical Science from the University of Technology Iraq-Baghdad in 1989 and 2003 respectively, and the Ph.D. degree in Electrical Engineering from The Montfort University, U.K. His area of interest includes of power electronics field and renewable energy. He can be contacted at email: 3705@uotechnology.edu.iq.